PHYSICAL REVIEW C, VOLUME 62, 061301(R)

Relativistic mean field description for the shears band mechanism in ^{84}Rb

Hideki Madokoro,[1,*] Jie Meng,[2,†] Masayuki Matsuzaki,[1,3,‡] and Shuhei Yamaji[1,§]
[1]*RI Beam Factory Project Office, RIKEN, Wako, Saitama 351-0198, Japan*
[2]*Department of Technical Physics, Peking University, Beijing 100871, China*
[3]*Department of Physics, Fukuoka University of Education, Munakata, Fukuoka 811-4192, Japan*
(Received 6 June 2000; published 2 November 2000)

For the first time, the relativistic mean field (RMF) model is applied to the shears band recently observed in $^{84}_{37}$Rb. Signals of the appearance of the shears mechanism, such as smooth decreases of the shears angle and of the $B(M1)/B(E2)$ ratio while keeping the nearly constant tilt angle, are well reproduced. Thus it is shown that the microscopic RMF model can nicely describe the shears band in this nucleus.

PACS number(s): 21.60.Jz, 21.60.Ev, 23.20.−g, 27.50.+e

Recently obtained data of the so-called shears bands in the proton rich Pb isotopes [1–5] are well described within the framework of the tilted axis cranking (TAC) [6–11] approach. In the shears bands, the magnetic dipole vector, which arises from few proton particles (holes) and few neutron holes (particles) in high-j orbitals, rotates around the total angular momentum vector. At the band head, the proton and neutron angular momenta are almost perpendicular. This coupling results in the total angular momentum which is tilted from the principal axes. With an increase of the rotational frequency, both the proton and neutron angular momenta align toward the total angular momentum. Consequently, the direction of the total angular momentum does not change so much and regular rotational bands are formed in spite of the fact that the density distribution of the nucleus is almost spherical or weakly deformed. These kinds of rotation are called magnetic rotation [9,12] in order to distinguish from the usual collective rotation in well-deformed nuclei (called electric rotation). Magnetic rotation has also been observed in other regions such as $A\sim 110$ [13–18] and 140 [19] regions. In a recent experiment, new shears bands in the Rb isotopes were discovered [20,21]. These are the first experimental data obtained in the $A\sim 80$ mass region. From the theoretical side, such shears bands have been well examined by the shell-model [22] and a model based on the mean field approximation [8]. The shell-model approach is especially suitable for those in the vicinity of doubly closed nuclei. When we add more and more particles to the doubly closed core, a transition from complicated multipletlike level structures to regular rotational bands in deformed nuclei is observed. Shears bands are seen in the middle region, that is, the system in which only a few proton particles/holes and a few neutron holes/particles are involved. The shell model can describe well both a multipletlike and a rotational-like structure, including the shears bands, as well as a transition from one structure to another structure.

A weak point of the shell-model approach is the effects coming from the truncation of the model space. As for the study of shears bands, it is suggested [22] that the polarization of the low-j orbitals (e.g., pf shells in the Pb isotopes) would have a ''glue'' role, which combines the outside high-j particles or holes to form a blade of shears. This is important for the bands to be stabilized. The truncated shell model may not be suitable to describe such effects properly because of the limitation of the model space. On the other hand, such polarization effects can be easily included in the mean field models as there is no limitation of the configuration space. It is difficult, however, to describe the multipletlike level structures and the transition from multipletlike to rotational-like structures in the simple mean-field approach. Therefore, complementary approaches, from both the shell-model and the mean-field models, are necessary in order to get a whole description of the property of the shears bands.

Focusing on the mean-field approaches to the shears bands, only studies based on the pairing+QQ Hamiltonian [8,3] have been done up to now. Those based on more sophisticated models, such as the Skyrme Hartree-Fock (SHF) and the relativistic mean field (RMF) models are still missing and strongly desired. In a previous preliminary work [23], we have applied the RMF model to the tilted axis rotation. In the present paper, we for the first time describe the shears bands by the RMF model, which has gratefully been successful in reproducing many properties of finite nuclei.

In the RMF model [24], we consider the following Lagrangian, which contains the nucleon and several kinds of meson fields, such as σ, ω, and ρ mesons, together with the photon fields (denoted by A) mediating the Coulomb interaction:

$$\mathcal{L}=\mathcal{L}_N+\mathcal{L}_\sigma+\mathcal{L}_\omega+\mathcal{L}_\rho+\mathcal{L}_A+\mathcal{L}_{\rm int}+\mathcal{L}_{{\rm NL}\sigma}\ ,$$

where $\mathcal{L}_{\rm int}$ is the interaction part between nucleons and mesons. The nonlinear self interactions among the σ mesons, $\mathcal{L}_{{\rm NL}\sigma}$, are also included.

For applications to rotating nuclei, the Lagrangian of the RMF model must be generalized into a uniformly rotating frame which rotates with a constant rotational frequency, $\mathbf{\Omega}=(\Omega_x,\Omega_y,\Omega_z)$. From this generalized Lagrangian, the equations of motion are derived. This can be done in the

*Electronic address: madokoro@postman.riken.go.jp
†Electronic address: mengj@pku.edu.cn
‡Electronic address: matsuza@fukuoka-edu.ac.jp
§Electronic address: yamajis@rikaxp.riken.go.jp

same manner as that in the principal axis cranking (PAC) case [25–28,23]. The resulting equations are

$$\left\{\boldsymbol{\alpha}\cdot\left(\frac{1}{i}\boldsymbol{\nabla}-g_\omega\boldsymbol{\omega}\right)+\beta(M-g_\sigma\sigma)+g_\omega\omega^0-\boldsymbol{\Omega}\cdot(\boldsymbol{L}+\boldsymbol{\Sigma})\right\}\psi_i = \epsilon_i\psi_i,$$

$$\{-\boldsymbol{\nabla}^2+m_\sigma^2-(\boldsymbol{\Omega}\cdot\boldsymbol{L})^2\}\sigma-g_2\sigma^2+g_3\sigma^3=g_\sigma\rho_s,$$

$$\{-\boldsymbol{\nabla}^2+m_\omega^2-(\boldsymbol{\Omega}\cdot\boldsymbol{L})^2\}\omega^0=g_\omega\rho_v,$$

$$\{-\boldsymbol{\nabla}^2+m_\omega^2-(\boldsymbol{\Omega}\cdot(\boldsymbol{L}+\boldsymbol{S}))^2\}\boldsymbol{\omega}=g_\omega\boldsymbol{j}_v,$$

where the ρ-meson and photon fields are omitted for simplicity, although they are included in the numerical calculation. It is known [27] that the Coriolis terms for the meson and photon fields (those proportional to Ω^2 in the above equations) give very small contributions and can be completely neglected. The method used to solve the coupled equations of motion is, again, the same as that in the PAC case. The nucleon and meson fields are expanded in terms of three-dimensional harmonic-oscillator eigenfunctions. Note that, contrary to the PAC case, the signature symmetry is broken in the TAC approach. The parity is thus the only symmetry we assume in our code. The cutoff parameters of the expansion are taken as $N_\mathrm{F}=10$ for nucleon fields and $N_\mathrm{B}=10$ for meson fields, respectively. When we increase these cutoff parameters to $N_\mathrm{F}=N_\mathrm{B}=12$, we find the changes of the calculated values are only 0.1% for the total energies, 2–3 % for the total quadrupole moments and 0.5% for the total angular momenta, respectively. As for the parameter set, we use that called NL3 [29]. In the present code, the pairing correlations are not taken into account. They should be included for a precise description of the properties of heavy and medium-heavy nuclei in the low spin region. In the relativistic case, however, the size of the Hamiltonian in the Hartree-Bogoliubov equation becomes twice as large as that of the nonrelativistic case due to the degrees of freedom of the lower components. This makes it very time consuming to perform a three-dimensional cranking calculation with pairing. Because this is the first RMF work for the shears bands, one of the important purposes of which is to examine its applicability to the shears bands, we here concentrate on the calculation without including the pairing interaction.

As the first example of our RMF calculation of the shears bands, we choose the nucleus $^{84}_{37}\mathrm{Rb}_{47}$. In all of our calculations, we assume that the proton configuration is fixed to be $\pi(pf)^7(1g_{9/2})^2$ with respect to the $Z=28$ magic number, that is, a pair of protons align into the $1g_{9/2}$ orbital. This alignment is important for the appearance of the shears bands, otherwise no tilted rotating state is observed. As for the neutron configuration, we assume $\nu(1g_{9/2})^{-3}$ with respect to the $N=50$ magic number. These assumptions lead to a rotational band with negative parity, which is consistent with the experimental observation. In order to find minima, we increase $\Omega=|\boldsymbol{\Omega}|$ with a step of 0.1 MeV, for each of which the minimum in the $\theta-\phi$ plane is searched. Our definition of the tilt angles is the same as that in Refs. [30,31],

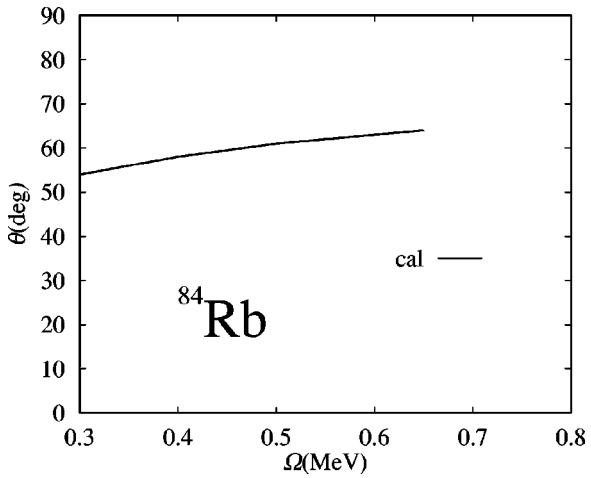

FIG. 1. Tilt angle θ as a function of the rotational frequency.

that is, $(\theta,\phi)=(90°,0°)$ corresponds to normal collective rotation around the x axis. This procedure is continued until $\Omega=0.6$ MeV. When we come to $\Omega=0.7$ MeV, another minimum appears at which the shape is almost spherical. This is consistent with the experimental observation of the up-bending seen in $J^{(2)}$ and $B(M1)/B(E2)$ (see Figs. 2 and 5 below), which may imply the occurrence of such crossing. Therefore we add $\Omega=0.65$ MeV to the mesh points of the frequency in our calculation and the results are shown only up to this frequency. Usually we should distinguish the tilt angles defined for the rotational frequency vector $\boldsymbol{\Omega}$ (denoted by θ_Ω and ϕ_Ω) from those defined for the angular momentum vector $\boldsymbol{J}$ (denoted by θ_J and ϕ_J). In this study, however, we are interested in only each minimum, where $\boldsymbol{\Omega}$ and $\boldsymbol{J}$ are parallel and therefore $(\theta_\Omega,\ \phi_\Omega)$ coincides with $(\theta_J,\ \phi_J)$, and so we simply denote them by (θ,ϕ). The deformations β_2 and γ are calculated from the quadrupole moments [32]. We find the deformation slightly decreases from $\beta_2\sim0.18$ at $\Omega=0.3$ MeV to $\beta_2\sim0.16$ at $\Omega=0.65$ MeV. These values are close to the fixed value used in the $P+QQ$ examination [20], that is, $\epsilon_2=0.14$. The triaxial deformation is at most a few degrees and rather small, which can be neglected. This simplifies our calculation because we can concentrate on the two-dimensional calculations, where ϕ are always set to 0°. Besides, we can restrict ourselves to only the range $\theta=0°-90°$ thanks to the D_2 symmetry [30,31].

Figure 1 shows how the tilt angle θ at the minima changes with respect to the rotational frequency. At low rotational frequencies, we find tilted minima appear at $\theta\gtrsim50°$. With an increase of Ω, the tilt angle slightly changes but always stays at $\theta\simeq55°-65°$.

In Fig. 2 the kinematical ($J^{(1)}$) and dynamical ($J^{(2)}$) moments of inertia are plotted. The experimental values are calculated from the transition energies by using the finite difference approximations for $\Delta I=1$ bands,

$$J^{(1)}=\frac{I}{E_\gamma(I\to I-1)}\ \text{ with }\ \Omega=E_\gamma(I\to I-1),$$

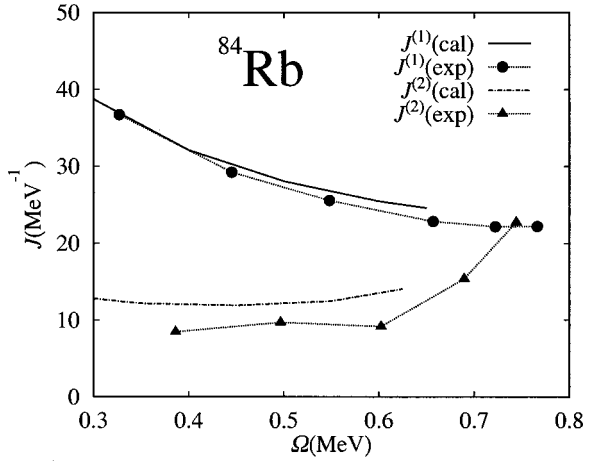

FIG. 2. Calculated kinematical ($J^{(1)}$) and dynamical ($J^{(2)}$) moments of inertia together with the experimental data taken from Ref. [20]. Solid and dot-dashed lines represent the calculated $J^{(1)}$ and $J^{(2)}$, respectively. Experimental data are shown by filled circles ($J^{(1)}$) and triangles ($J^{(2)}$) connected by dotted lines.

$$J^{(2)}=\frac{1}{E_\gamma(I+1\rightarrow I)-E_\gamma(I\rightarrow I-1)}$$

$$\text{with}\quad \Omega=\frac{E_\gamma(I+1\rightarrow I)+E_\gamma(I\rightarrow I-1)}{2}.$$

$J^{(2)}$ does not change so much up to $\Omega\sim 0.6$ MeV. Experimental data show an increase of $J^{(2)}$ above this frequency. This might be caused by a crossing as mentioned before. Although the calculated $J^{(2)}$ is slightly too large, as a whole both moments of inertia are well reproduced. Small discrepancies seen in Fig. 2 may be cured by including the pairing correlation.

Figure 3 shows how the direction of the total angular momentum vector changes with an increase of the rotational frequency. Also shown are the net contributions from protons and neutrons individually. Because we assume no core in our calculation, $\boldsymbol{J}_\pi$ and $\boldsymbol{J}_\nu$ are here defined as the contributions from *all* particles below the Fermi level,

$$\boldsymbol{J}_\pi=\sum_{i=1}^{Z}\langle\hat{\boldsymbol{J}}\rangle_i,$$

$$\boldsymbol{J}_\nu=\sum_{i=1}^{N}\langle\hat{\boldsymbol{J}}\rangle_i,$$

$$\boldsymbol{J}_{\rm tot}=\boldsymbol{J}_\pi+\boldsymbol{J}_\nu,$$

$$|\boldsymbol{J}_{\rm tot}|\equiv\sqrt{I(I+1)}.$$

We find, however, almost all contributions come from two proton particles and three neutron holes in the $1g_{9/2}$ orbital. Several proton particles in the lower (pf) orbitals also give substantial contributions to the proton angular momentum. Because of this, $\boldsymbol{J}_\pi$ has not only a large J_x component but also a substantial J_z component even at lower frequencies. As the frequency increases, we can see that the shears angles decrease while keeping the direction of the total angular momentum with nearly constant tilt angle. This is explicitly shown in Fig. 4. Here the shears angles Θ_π, Θ_ν, and $\Theta_{\rm tot}$ are calculated from the following semiclassical expressions:

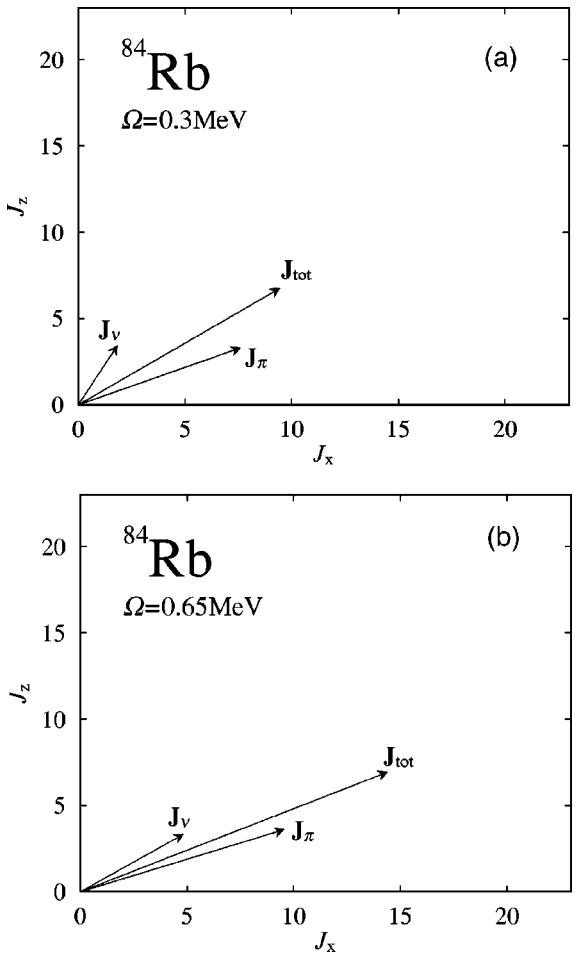

FIG. 3. Composition of the total angular momentum at $\Omega=0.3$ MeV (a) and 0.65 MeV (b). $\boldsymbol{J}_\pi$ and $\boldsymbol{J}_\nu$ represent the contributions from protons and neutrons, respectively. $\boldsymbol{J}_{\rm tot}$ is the total angular momentum. The angle between $\boldsymbol{J}_{\rm tot}$ and the J_z axis coincides with the tilt angle θ (see Fig. 1).

$$\cos\Theta_\pi=\frac{\boldsymbol{J}_\pi\cdot\boldsymbol{J}_{\rm tot}}{|\boldsymbol{J}_\pi||\boldsymbol{J}_{\rm tot}|},\qquad \cos\Theta_\nu=\frac{\boldsymbol{J}_\nu\cdot\boldsymbol{J}_{\rm tot}}{|\boldsymbol{J}_\nu||\boldsymbol{J}_{\rm tot}|},$$

$$\Theta_{\rm tot}=\Theta_\pi+\Theta_\nu.$$

Clearly our result shows almost linear decreases of Θ_π, Θ_ν, and $\Theta_{\rm tot}$. We thus have observed that the shears mechanism does appear.

Another quantity considered as a signal of the shears mechanism is the ratio of $B(M1)$ to $B(E2)$ [33]. A smooth decrease of the $B(M1)/B(E2)$ ratio is expected in the shears bands [8,9]. These transition probabilities are calculated

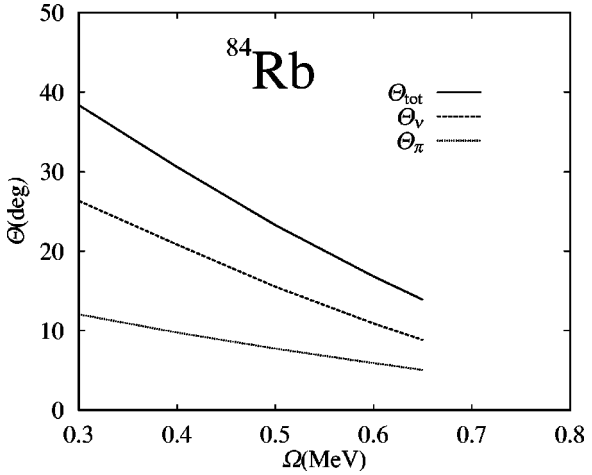

FIG. 4. The shears angles Θ_π, Θ_ν, and $\Theta_{\rm tot}$. Θ_π is the angle between $\boldsymbol{J}_\pi$ and $\boldsymbol{J}_{\rm tot}$, Θ_ν between $\boldsymbol{J}_\nu$ and $\boldsymbol{J}_{\rm tot}$, and $\Theta_{\rm tot}$ between $\boldsymbol{J}_\pi$ and $\boldsymbol{J}_\nu$.

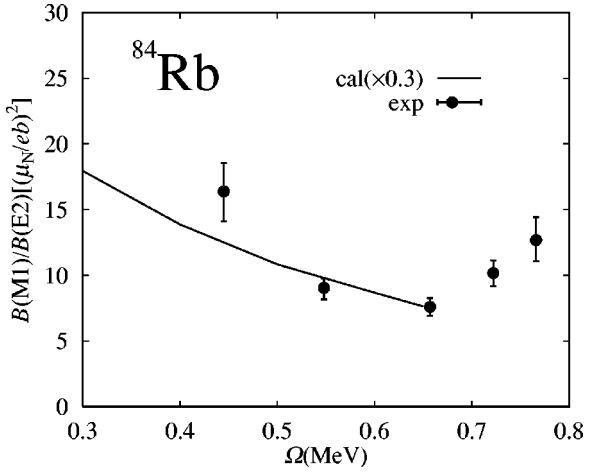

FIG. 5. The ratio of $B(M1)$ to $B(E2)$ as a function of the rotational frequency. The calculated value is multiplied by 0.3. Experimental data are taken from Ref. [20].

from the semiclassical expressions [30]. For $B(M1)$, we must calculate the magnetic moments,

$$\boldsymbol{\mu}=g_l \sum_{i=1}^{N \text{ or } Z} \langle \hat{\boldsymbol{L}} \rangle_i + g_s^{(\rm eff)} \sum_{i=1}^{N \text{ or } Z} \langle \hat{\boldsymbol{S}} \rangle_i ,$$

separately for protons and neutrons. As for the g factors we use the standard values [34]; $g_l=1$, $g_s=5.58$ for protons and $g_l=0$, $g_s=-3.82$ for neutrons, respectively. Note that the effective spin g factor ($g_s^{(\rm eff)}$) is equal to the free spin g factor multiplied by 0.7. We do not introduce the effective charge for $B(E2)$ because our calculation is a fully microscopic one.

Figure 5 shows the $B(M1)/B(E2)$ ratio. The calculated result is attenuated by a factor of 0.3, because only the Ω dependence is reliable in the present calculation due to the following reasons.

(1) In our results the effect of the pairing interaction is not taken into account. As for $B(M1)$, almost all contributions come from the valence particles/holes, while in the case of $B(E2)$ the contribution from the ''core'' part is rather large. Because the pairing correlation strongly affects the levels near the Fermi level, $B(M1)$ is largely affected by including the pairing correlation, while $B(E2)$ is not. In our case of ^{84}Rb, the tendency that proton particles in the low-k levels favor the x axis (rotational aligned) and neutron holes in the high-k levels favor the z axis (deformation aligned) might be smeared out to some extent by including the pairing, because the pairing mixes many levels. This can cause the decrease of the shears angle, and then $B(M1)$ would be reduced. Thus we can expect that including the pairing will reduce the $B(M1)/B(E2)$ ratio.

(2) The particle-vibration coupling calculations based on the RPA show that the in-band $B(M1)/B(E2)$ values are reduced if the gamma vibration is collective enough [35] because it introduces wobbling and consequently the overlap between the initial and the final states of the transition is reduced. This would apply also to the present case, as the $P+QQ$ result [20] suggests that ^{84}Rb is a gamma-soft nucleus.

The tendency of a smooth decrease of $B(M1)/B(E2)$ up to $\Omega \sim 0.65$ MeV is well reproduced as can be seen from Fig. 5. Thus our calculation can again show the appearance of the shears bands.

To summarize, we have applied the RMF model to the newly discovered shears band in ^{84}Rb. To this time only studies based on the $P+QQ$ Hamiltonian had been performed for the mean field approach to the shears bands. This is the first examination which is based on a more sophisticated mean field model. Our RMF calculation shows decreases of the shears angles and the $B(M1)/B(E2)$ ratio as the frequency increases, while keeping nearly constant tilt angle. Thus we could reproduce the appearance of the shears mechanism in this nucleus.

Finally, we comment on the case of ^{82}Rb, in which a shears band is also observed. Unfortunately, we could not reproduce the shears band so definitely for ^{82}Rb. A possible reason is as follows: In the calculation of ^{82}Rb without pairing, two additional holes must be created compared with ^{84}Rb, that is, there exist five neutron holes with respect to the $N=50$ magic number. It seems that one of these additional two holes strongly favors $\theta=90°$, and therefore works in the direction of shifting the angular momentum vector toward $\theta=90°$. Pairing would reduce this effect.

In the $A\sim 80$ region, several high-K bands have been observed [36]. It remains unsolved, however, whether these are really shears bands or usual high-K bands in the well-deformed nuclei. In the future, we will examine other isotopes in this region, after including the pairing correlation, to clarify the above question.

One of us (J.M.) thanks the hospitality of the Cyclotron Center, RIKEN where part of this work was done. His work was also partly supported by the Major State Basic Research Development Program Under Contract No. G2000077407 and the National Natural Science Foundation of China (Contracts No. 19847002 and 19935030).

[1] R. M. Clark *et al.*, Phys. Lett. B **275**, 247 (1992); Phys. Rev. Lett. **78**, 1868 (1997).
[2] G. Baldsiefen *et al.*, Phys. Lett. B **275**, 252 (1992); Nucl. Phys. **A587**, 562 (1995); **A592**, 365 (1995); Phys. Rev. C **54**, 1106 (1996); Z. Phys. A **355**, 337 (1996).
[3] G. Baldsiefen *et al.*, Nucl. Phys. **A574**, 521 (1994).
[4] M. Neffgen *et al.*, Nucl. Phys. **A595**, 499 (1995).
[5] H. Hübel *et al.*, Z. Phys. A **358**, 237 (1997); Prog. Part. Nucl. Phys. **38**, 89 (1997).
[6] A. K. Kerman and N. Onishi, Nucl. Phys. **A361**, 179 (1981); T. Horibata and N. Onishi, Phys. Lett. B **325**, 283 (1994); Nucl. Phys. **A596**, 251 (1994).
[7] S. Frauendorf and T. Bengtsson, in *Future Directions in Nuclear Physics with 4π Gamma Detection Systems of the New Generation*, Strasbourg, France, 1991, edited by J. Dudek and B. Haas, AIP Conf. Proc. No. 259 (AIP, New York, 1992), p. 223; F. Dönau and S. Frauendorf, in *Proceedings of the International Symposium on Nuclear Physics of our Times*, Sanibel Island, FL, 1992, edited by A. V. Ramayya (World Scientific, Singapore, 1993), p. 411.
[8] S. Frauendorf, Nucl. Phys. **A557**, 259c (1993).
[9] S. Frauendorf, J. Meng, and J. Reif, in Proceedings of the Conference on Physics from Large γ-Ray Detector Arrays, edited by M. A. Deleplanque, California, 1994, Report LBL-35687, Vol. II, p. 52.
[10] S. Frauendorf and J. Meng, Z. Phys. A **356**, 263 (1996).
[11] S. Frauendorf, nucl-th/0005025.
[12] S. Frauendorf, Z. Phys. A **358**, 163 (1997).
[13] A. Gadea *et al.*, Phys. Rev. C **55**, R1 (1997); Z. Phys. A **358**, 193 (1997).
[14] R. S. Chakrawarthy *et al.*, Phys. Rev. C **55**, 155 (1997).
[15] P. Vaska *et al.*, Phys. Rev. C **57**, 1634 (1998).
[16] D. G. Jenkins *et al.*, Phys. Lett. B **428**, 23 (1998); Phys. Rev. Lett. **83**, 500 (1999).
[17] R. M. Clark *et al.*, Phys. Rev. Lett. **82**, 3220 (1999).
[18] N. S. Kelsall *et al.*, Phys. Rev. C **61**, 011301(R) (2000).
[19] F. Brandolini *et al.*, Phys. Lett. B **388**, 468 (1996).
[20] R. Schwengner *et al.*, in *ENAM 98, Exotic Nuclei and Atomic Masses*, Bellaire, MI, 1998, edited by Bradley M. Sherrill, David J. Morrissey, and Cary N. Davids, AIP Conf. Proc. No. 455 (AIP, Woodbury, NY, 1998), p. 594; H. Schnore *et al.*, Phys. Rev. Lett. **82**, 4408 (1999).
[21] J. Döring, D. Ulrich, G. D. Johns, M. A. Riley, and S. L. Tabor, Phys. Rev. C **59**, 71 (1999).
[22] S. Frauendorf, J. Reif, and G. Winter, Nucl. Phys. **A601**, 41 (1996).
[23] H. Madokoro, J. Meng, M. Matsuzaki, and S. Yamaji, Proceedings of the International Symposium on Models and Theories of the Nuclear Mass, RIKEN, 1999 [RIKEN Rev. **26**, 126 (2000)].
[24] For recent reviews see, P. Ring, Prog. Part. Nucl. Phys. **37**, 193 (1996); B. D. Serot and J. D. Walecka, Int. J. Mod. Phys. A **6**, 515 (1997).
[25] W. Koepf and P. Ring, Nucl. Phys. **A493**, 61 (1989); **A511**, 279 (1990); J. König and P. Ring, Phys. Rev. Lett. **71**, 3079 (1993).
[26] K. Kaneko, M. Nakano, and M. Matsuzaki, Phys. Lett. B **317**, 261 (1993).
[27] A. V. Afanasjev, J. König, and P. Ring, Nucl. Phys. **A608**, 107 (1996).
[28] H. Madokoro and M. Matsuzaki, Phys. Rev. C **56**, R2934 (1997).
[29] G. A. Lalazissis, J. König, and P. Ring, Phys. Rev. C **55**, 540 (1997).
[30] S. Frauendorf and J. Meng, Nucl. Phys. **A617**, 131 (1997).
[31] S. Ohtsubo and Y. R. Shimizu, Prog. Theor. Phys. **98**, 1099 (1997).
[32] A. V. Afanasjev, J. König, and P. Ring, Phys. Lett. B **367**, 11 (1996).
[33] F. Dönau, Nucl. Phys. **A471**, 469 (1987).
[34] Å. Bohr and B. Mottelson, *Nuclear Structure*, Vol. I (Benjamin, New York, 1969).
[35] M. Matsuzaki, Y. R. Shimizu, and K. Matsuyanagi, Prog. Theor. Phys. **79**, 836 (1988).
[36] S. L. Tabor and J. Döring, Phys. Scr. **T56**, 175 (1995).